The Effect of Yarn Hairiness on Air Drag in Ring Spinning

Zheng-Xue Tang, Xungai Wang, and Lijing Wang

School of Engineering and Technology, Deakin University,

Geelong, VIC 3217, Australia

W. Barrie Fraser

School of Mathematics and Statistics, The University of Sydney,

Sydney, NSW 2006, Australia

ABSTRACT

Air drag on yarn and package surfaces affects yarn tension, which in turn affects energy consumption and ends-down in ring spinning. This paper investigates the effects of yarn hairiness on air drag in ring spinning. Theoretical models of skin friction coefficient on the surface of rotating yarn packages were developed. The predicted results were verified with experimental data obtained from cotton and wool yarns. The results show that hairiness increases the air drag by about one quarter and one third for the rotating cotton and wool yarn packages respectively. In addition, yarn hairiness increases the air drag by about one tenth on a ballooning cotton yarn.

Keywords: Ring spinning, Ballooning yarn, Yarn package, Yarn hairiness, Air drag

1. Introduction

Ring spinning has been a very important technology for staple yarns as it produces relatively high quality yarns and the quality of ring spun yarns has been used as the benchmark for yarns spun on other systems [24]. Many researchers have made contributions to development of ring spinning system to reduce power consumption and improve productivity [5, 7, 9, 11–17, 19–23, 25, 26]. In particular, the effect of air drag on spinning tension, which relates to ends-down and energy consumption, has been reported [6, 10, 27, 38, 39]. However, for simplification of calculation and modeling, previous studies often neglected yarn hairiness and used smooth filament yarns.

The concept of hairiness as a quantitative parameter of yarns was first definitively stated in the early 1950's [2]. Since then yarn hairiness and its measurement have attracted increasing attention. In the last two decades, considerable research has gone into the methods of measuring and reducing yarn hairiness [3, 4, 29–35, 37]. Recently, Chang *et al*. [8] reported the importance of hair length and number of hairs in determining the power consumption to rotate a ring spun yarn package.

This paper will study the effects of hairiness on air drag in ring spinning. Figure 1 displays the ring spinning process, which shows that the effects of yarn hairiness on air drag are mainly in two parts – the surface of a rotating yarn package and the balloon. We will first test the hairiness effects, and then develop the models of skin friction coefficient on the surface of rotating cotton and wool yarn packages. Finally, we will verify the results empirically.

2. Experimental

2.1 Yarn samples and their hairiness indexes

We used a 38 tex cotton yarn and a 103 tex wool yarn in the experiments. We measured the hairiness index of these two yarns on an Uster Tester 4 under standard conditions and at a speed of 400 m/min. Table 1 lists the hairiness results, which we will use for further analyses in the following sections.

Table 1 Hairiness index of cotton and wool yarns

Yarn type	Cotton	Wool
Yarn count (tex)	38	103
Hairiness index (H)	8.1	13.0

2.2 Power consumption on rotating yarn package surfaces

We adopted a single spindle rig (see Figure 3 in Ref. [8]) to measure the level of power consumption during the rotation of a single yarn package. We used the roving build method and the 38 tex cotton yarn to wind three yarn packages with different layers (i.e., package *A* with 2 layers, package *B* with 7 layers and package *C* with 12 layers) and the 103 tex pure wool yarn to wind one package (i.e., package *D* with 2 layers). The packages have the same height h of 0.245 m. After winding the packages, we measured the package diameters. For each of the four packages, we took the diameter measurements at two ends and in the middle, and used their average as the diameter of the package. The cotton yarn packages have average diameters d_1 of

0.0279 m, d_2 of 0.0302 m, d_3 of 0.0325 m, and the pure wool yarn package has diameter d_4 of 0.0297 m.

We tested each of the four packages twice at spindle speeds ranging from 2,000 rpm (i.e. 33 rps) to 16,000 rpm (i.e. 267 rps), in steps of 2000 rpm. For each of the packages at different spindle speeds, we took the average values of the current and voltage reading from the test device and used these readings to calculate the power consumption at a given spindle speed. The experimental results are shown in Table 2.

Table 2 Power consumption on the surfaces of rotating yarn packages at varying spindle speed

Spindle speed		Package A	Package B	Package C	Package D	Empty bobbin
[rpm]	[rps]	[W]	[W]	[W]	[W]	[W]
2000	3	15.939	18.892	22.196	25.771	5.138
4000	67	20.581	23.547	26.898	28.676	9.744
6000	100	26.964	29.947	33.398	33.929	15.729
8000	133	34.987	38.273	42.410	41.993	22.847
10000	167	44.951	48.515	52.496	52.288	31.771
12000	200	55.675	59.425	63.427	62.412	42.055
14000	233	69.865	73.896	78.464	76.752	55.567
16000	267	86.359	90.612	95.130	93.390	71.431

2.3 Tension in a ballooning yarn

We used the 38 tex cotton yarn and the roving build method to wind a yarn package with one layer and removed the hairiness on the package surface by singeing. Then we got the singed 38 tex cotton yarn by unwinding the yarn from the package. We measured tension in the singed and un-singed yarns using a specially constructed rig

(see Figure 2 in Ref. [28]). One end of the yarn, which passes through the guide-eye, is attached to the tension sensor and another end is fixed on the eyelet. When the eyelet starts rotating, the yarn between the guide-eye and rotating eyelet will form a balloon and generate tension in the yarn. The tension signal at the guide-eye is digitized by the computer data acquisition system.

3. Theoretical

3.1 Modelling skin friction coefficient on a yarn package surface

The power required to overcome skin friction drag, P_f [W], on the surface of a rotating yarn package can be expressed as

$$P_f = \frac{1}{2}\rho(\pi d V)^3 S_p C_f \qquad (1)$$

where C_f [scalar] is the skin friction coefficient on the package surface, V [rps] is a given full spindle speed, d [m] is the diameter and S_p [m^2] is the surface-area of the yarn package [27].

During yarn winding in ring spinning, the package profile varies with winding-on time and is not of a strictly cylindrical shape. For a full yarn package, the surface area of the main part (with the maximum package diameter) is about 90% of the yarn package surface. In order to simplify the calculation, we consider the skin friction coefficient on the surface of the yarn package to be the skin friction coefficient on the surface of the main part of this yarn package. Let d [m] be the diameter of main part

of a yarn package, then we can take the yarn package as a cylinder having diameter d and height h [m], and Equation 1 becomes

$$C_f = \frac{2P_f}{\rho(d\pi)^4 hV^3} \tag{2}$$

Based on the experimental data in Table 2, we calculated the skin friction coefficient on the surface of natural cotton yarn package with a diameter of 0.0279 m (i.e., package *A*) using Equation 2, as shown in the right column in Table 3. With the same method, we can calculate the skin friction coefficient on the surface of other yarn packages.

Table 3 Skin friction coefficients on the surfaces of natural yarn package and singed yarn package (package diameter = 0.0279 *m*)

Spindle speed (V)		Skin friction coefficient (C_f) on package surfaces [scalar]	
[rpm]	[rps]	Hairiness Singed*	Natural hairiness
2000	33	16.9321	33.5594
4000	67	2.6666	4.2088
6000	100	0.9333	1.2929
8000	133	0.4469	0.5894
10000	167	0.2539	0.3276
12000	200	0.1608	0.1959
14000	233	0.1090	0.1295
16000	267	0.0778	0.0906

* Data obtained from [27].

The skin friction coefficient (C_f [scalar]) on a rotating yarn package surface without hairiness depends on the full spindle speed (V [rps]) and the package diameter (d [m]):

$$C_f = \frac{0.025}{d} a V^b \tag{3}$$

where a and b are constants which can be determined from experiments [27].

We modified Equation 3 into a general model for skin friction coefficient on the surface of a rotating yarn package:

$$C_f = \frac{0.025}{d}\left(a V^b + a_1 H V^{b_1}\right) \tag{4}$$

where H [scalar] is yarn hairiness index which can be measured, a, b, a_1 and b_1 are constants which can be determined from experiments.

If we apply Equation 4 to a rotating yarn package surface without hairiness (e.g. H = 0), then Equation 4 becomes Equation 3. In Equation 3, the constants (a = 148030 and b = –2.575) for the cotton yarn were determined in the previous work [27]. Now we will determine constants a_1 and b_1 using experimental data.

From Table 1, the Hairiness index of cotton 38 tex yarn is 8.1. Based on the data in the second and fourth columns (from left to right) in Table 3 and using the principle of making a "best fit" between the theoretical and experimental points, as shown in Figure 2, we obtained a_1 = 384128 and b_1 = -3.4316 for the cotton yarn in Equation 4.

The comparison of skin friction coefficients on the surface of yarn packages between experiments and prediction from Equation 4 is shown in Table 4.

Table 4 Comparison of skin friction coefficients on yarn package surfaces between experiments and predictions

Spindle speed (V)	Cotton yarn package B (d = 0.0302 m, H = 8.1)		Cotton yarn package C (d = 0.0325 m, H = 8.1)		Wool yarn package D (d = 0.0297 m, H = 13.0)	
[rps]	$C_{f\text{-experimental}}$	$C_{f\text{-theoretical}}$	$C_{f\text{-experimental}}$	$C_{f\text{-theoretical}}$	$C_{f\text{-experimental}}$	$C_{f\text{-theoretical}}$
33	31.1931	29.9952	28.9007	27.8724	50.1366	42.4932
67	3.9130	3.8834	3.6329	3.6086	5.7505	5.1327
100	1.1943	1.2205	1.1088	1.1341	1.6379	1.5522
133	0.5467	0.5451	0.5179	0.5065	0.7269	0.6761
167	0.3038	0.2940	0.2809	0.2732	0.3988	0.3582
200	0.1824	0.1783	0.1676	0.1657	0.2290	0.2144
233	0.1212	0.1172	0.1131	0.1089	0.1501	0.1394
267	0.0850	0.0816	0.0784	0.0758	0.1042	0.0963

Note: d – the diameter of a yarn package; H – the hairiness index of a yarn.

3.2 Modelling air drag coefficient on a ballooning yarn

We consider yarn tension at a material point $\boldsymbol{P}(r, \theta, z)$ for a free-balloon (no control ring) spinning, as shown in Figure 3. Let $\boldsymbol{F}_d$ be the air drag, the quantity of air drag acting on the yarn segment ds at $\boldsymbol{P}$ on a ballooning yarn owing to air-resistance can be evaluated by [8]

$$\Delta F_d = \frac{1}{2}\Delta C_D \bullet \rho \bullet \Delta A \bullet \upsilon^2 \tag{5}$$

where ΔF_d [N] = $|\Delta \boldsymbol{F}_d|$, ρ [kg/m^3] is air density, ΔC_D [scalar] is the drag coefficient at $\boldsymbol{P}$, ΔA [m^2] is the projected frontal area of the yarn segment ds, i.e., ΔA = yarn diameter × the length of ds, and υ [m/s] is the linear velocity of the ballooning yarn at $\boldsymbol{P}$.

Since the velocity at point ***P*** on the ballooning yarn depends on the balloon radius at ***P*** and the rotational speed of the yarn which is constant, the drag coefficient at ***P*** depends on the yarn velocity at ***P***. Therefore, ΔC_D and υ vary with balloon radius.

For simplicity, however, we assume that the air drag coefficient ΔC_D is constant along the whole length of the yarn in the balloon, and it takes on a value appropriate to the velocity of the yarn at the maximum balloon radius. From Equation 5, the quantity of air drag acting on the whole ballooning yarn can be estimated by

$$F_d \approx 2\pi^2 \rho d_y s_l r_{\max}^2 V^2 C_D \qquad (6)$$

where ρ = 1.197 kg/m^3, d_y [m] is yarn diameter, s_l [m] is yarn length in balloon, $r_{\max}$ [m] is the maximum radius of the balloon, V [rps] is spindle speed and C_D [scalar] is air drag coefficient on the ballooning yarn.

From Equation 6, we can estimate the effects of yarn hairiness on air drag, (i.e., the percentage of air drag increased due to yarn hairiness) on a ballooning yarn once we know air drag coefficients of the natural (hairy) yarn and the singed (hair free) yarn of the same diameter.

Figure 4 shows the comparisons of the curves of tension at guide-eye against yarn-length in balloon, where the experimental data came from simulated spinning experiments and have been converted into a normalized form, and the theoretical curve came from simulation with normalized air drag coefficients, which have been

estimated by making a "best fit" between the theoretical and experimental turning points. The normalized air drag coefficient p_0 equals 5.0 for the natural 38 tex cotton yarn and p_0 equals 4.6 for singed 38 tex cotton yarn.

There is a relationship between the normalization form (p_0 [scalar]) and dimensional form (C_D [scalar]) of the air drag coefficient on a rotating yarn as below

$$C_D = \frac{m}{8\rho da} p_0 \tag{7}$$

where ρ = 1.197 kg/m^3, d [m] is yarn diameter, a [m] is ring radius and m [kg/m] is linear density of yarn [10].

4. Results and Discussion

4.1 Difference in hairiness effect on wool and cotton yarn package surfaces

The data in Table 3 show that the effect of yarn hairiness on skin friction coefficient on the surface of a rotating yarn package is inversely proportional to spindle speed. Specifically, the skin friction coefficient increases about 98% at spindle speed of 2000 rpm and about 16.5% at spindle speed of 16000 rpm for cotton yarn package.

Table 4 shows that the results from Equation 4 were verified by experimental data very well for cotton yarn packages *B* and *C* (e.g., the average relative error is less than 2.3%). However, for wool yarn package *D*, the experimentally determined skin friction coefficients were greater than those calculated from Equation 4 and the average relative error is about 10%. One reason for this may be that the hair fibers on

the wool yarn are much coarser and longer than the hair fibers on the cotton yarn (e.g., the average diameter of wool fibers is about 24 μm while the average width of cotton fibers is about 13 μm).

We modified Equation 4 into a new model which can more accurately predict skin friction coefficient on the surface of a rotating wool yarn package as below

$$C_f = \frac{0.025}{d}\left(aV^b + 1.4a_1 HV^{b_1}\right) \qquad (4a)$$

where d [m] is the diameter of a wool yarn package, V [rps] is a given full spindle speed, H[scalar] is the hairiness index of the wool yarn, a, b, a_1 and b_1 are still equal to 148030, –2.575, 384128 and -3.4316, respectively.

Figure 5 displays a comparison of skin friction coefficients on the surface of wool yarn package between experiments and model prediction from Equation 4*a*.

4.2. Effects of yarn hairiness on air drag on a rotating yarn package surface

A yarn package, being a circular-cylinder with diameter of d [m] and height of h [m], rotates at a given full spindle speed V [rps], the air drag F_d [N] on the package surface can be obtained by [1]

$$F_d = \frac{1}{2}\rho(\pi dV)^2 S_p C_f \qquad (8)$$

where ρ = 1.197 kg/m^3, S_p [m^2] is surface area and C_f [scalar] is skin friction coefficient on the surface of the circular-cylinder.

Let C_{fs} and F_{ds} be the skin friction coefficient and air drag, respectively, on the package surface of singed yarn; similarly, let C_{fn} and F_{dn} be the skin friction coefficient and air drag, respectively, on the package surface of un-singed natural yarn. We consider two cotton yarn packages wound by the 38 tex cotton yarn and another two wool yarn packages wound by the 103 tex wool yarn. All of the four packages have the same diameter of 0.045 m and the same height of 0.245 m, and the surfaces of one cotton package and one wool package were singed. Table 5 is a comparison of air drag for the singed and un-singed cotton yarn packages rotating at different speed, where C_{fs} was calculated from Equation 3, C_{fn} was calculated from Equation 4, F_{ds} and F_{dn} were calculated from Equation 8. Table 6 lists similar results for the wool yarn packages.

Table 5 Comparison of air drag between packages of natural and singed cotton yarns at different rotating speeds

Spindle speed (V)		Natural package surface		Surface without hairiness		$(F_{dn} - F_{ds})/F_{ds}$
[rpm]	[rps]	C_{fn} [scalar]	F_{dn} [N]	C_{fs} [scalar]	F_{ds} [N]	[%]
2000	33	20.1301	9.2667	9.8552	4.5367	51
4000	67	2.6062	4.7989	1.6539	3.0454	37
6000	100	0.8191	3.3934	0.5822	2.4121	29
8000	133	0.3658	2.6944	0.2776	2.0444	24
10000	167	0.1973	2.2705	0.1562	1.7982	21
12000	200	0.1197	1.9830	0.0977	1.6192	18
14000	233	0.0786	1.7736	0.0657	1.4819	16
16000	267	0.0548	1.6133	0.0466	1.3724	15

Table 6 Comparison of air drag between packages of natural and singed wool yarns at different rotating speeds

Spindle speed (V)		Natural package surface		Surface without hairiness		$(F_{dn} - F_{ds})/F_{ds}$
[rpm]	[rps]	C_{fn} [scalar]	F_{dn} [N]	C_{fs} [scalar]	F_{ds} [N]	[%]
2000	33	24.2400	11.1586	9.8552	4.5367	59
4000	67	2.9871	5.5003	1.6539	3.0454	45
6000	100	0.9138	3.7860	0.5822	2.4121	36
8000	133	0.4011	2.9544	0.2776	2.0444	31
10000	167	0.2137	2.4594	0.1562	1.7982	27
12000	200	0.1284	2.1285	0.0977	1.6192	24
14000	233	0.0838	1.8903	0.0657	1.4819	22
16000	267	0.0580	1.7097	0.0466	1.3724	20

Tables 5 and 6 show that yarn hairiness contributes 25% air drag (average value) on the surface of a rotating cotton yarn package and 35% air drag (average value) on the surface of a rotating wool yarn package.

4.3 Effect of yarn hairiness on air drag on a ballooning yarn

Let C_{Ds} and F_{ds} be the air drag coefficient and air drag, respectively, on a ballooning yarn which has been singed; similarly, let C_{Dn} and F_{dn} be the respective air drag coefficient and air drag on a ballooning natural yarn. If we ignore the effects of hairiness on the diameter and mass of yarn in balloon, from Equation 6,

$$F_{dn} = 2\pi^2 \rho d_y s_l r_{\max}^2 V^2 C_{Dn} \tag{9}$$

and

$$F_{ds} = 2\pi^2 \rho d_y s_l r_{\max}^2 V^2 C_{Ds} \tag{10}$$

where ρ = 1.197 kg/m^3, d_y [m] is yarn diameter, s_l [m] is yarn length in balloon, $r_{\max}$ [m] is the maximum radius of the balloon, V [rps] is spindle speed and C_D [scalar] is air drag coefficient on the ballooning yarn.

From Equations 7, 9 and 10, and p_{0n} = 5.0 and p_{0s} = 4.6 for the 38 tex cotton yarn, we have

$$(F_{dn} - F_{ds})/F_{ds} = \frac{C_{Dn} - C_{Ds}}{C_{Ds}} = \frac{p_{0n} - p_{0s}}{p_{0s}} \approx 8.7\ \% \qquad (11)$$

Equation 11 shows that the hairiness on a ballooning cotton yarn increases the air drag by around 9%. This can be considered to be skin friction drag increase due to hairiness when we ignore the effects of hairiness on the diameter and mass of yarn in balloon.

5. Conclusion

Models for predicting skin friction coefficient on the surface of rotating cotton and wool yarn packages are developed. The effects of yarn hairiness on air drag on the surface of a rotating yarn package and on a ballooning yarn are examined. The results indicate that -

(i) the effect of yarn hairiness on skin friction coefficient on the surface of a rotating yarn package is inversely proportional to spindle speed; specifically, for the cotton yarn package, the skin friction coefficient

increases from about 16% at a spindle speed of 16000 rpm to about 98% at a spindle speed of 2000 rpm;

(ii) the air drag on a ballooning yarn and the average air drag on the surface of a rotating yarn package both increase with an increase in yarn hairiness. For instance, singing the surface hairs off the cotton and wool yarn packages reduced the average air drag on the rotating packages by about 26% and 33% respectively; similarly, air drag on the ballooning cotton yarn reduced by about 9% when the yarn was singed to remove surface hairs.

This research highlights the significance of yarn hairiness in ring spinning. Realistic models of ring spinning should incorporate the effect of yarn hairiness on air drag acting on the rotating package surface as well as on the ballooning yarn.

Acknowledgment

This work was funded by a grant from the Australian Research Council (ARC) under its discovery project scheme. We would like to thank Mr. Chris Hurren at Deakin University for assisting with the experimental work.

Literature Cited

[1] Anderson, J. D., "Fundamentals of aerodynamics", 3rd ed., McGraw-Hill, Inc., 2001, p. 821.

[2] Barella, A., Yarn Hairiness, *Text. Prog*. **13**(1), 1–61 (1983).

[3] Barella, A., The Hairiness of Yarns, *Text. Prog*. **24**(3), 1–49 (1993).

[4] Barella, A., Yarn Hairiness Update, *Text. Prog*. **26**(4), 1–31 (1997).

[5] Batra, S. K., Ghosh, T. K and Zeidman, M. I., An integrated approach to dynamic analysis of the ring spinning process – part I: Without air drag and coriolis acceleration", *Textile Res. J.* **59**(6), 309–317 (1989).

[6] Batra, S. K., Ghosh, T. K., and Zeidman, M. I., An integrated approach to dynamic analysis of the ring spinning process – part II: With air Drag, *Textile Res. J.* **59**(7), 416–424 (1989).

[7] Batra, S. K., Ghosh, T.K., Zeng, Q., Robert, K.Q., and Fraser, W.B., An integrated approach to dynamic analysis of the ring spinning process – Part IV: Inherent Instability of the free balloon, *Textile Res. J.* **65**(7), 417–423 (1995)

[8] Chang, L., Tang, Z. X., and Wang, X., The effect of yarn hairiness on energy consumption in rotating a ring-spun yarn package, *Textile Res. J.* **73**(11), 949–954 (2003).

[9] Fan, R., Singh, S. K., and Rahn, C. D., Modal analysis of ballooning strings with small curvature, *Transactions of the ASME*, Vol. **68**, 332–338 (2001).

[10] Fraser, W. B., Air drag and friction in the two-for-one twister: results from the theory, *Journal of the Textile Institute*, **84**(3) 364–375 (1993).

[11] Fraser, W. B., On the theory of ring spinning, *Phil. Trans. R. Soc. Lond.* A, (Philosophical Transactions: Physical Sciences and Engineering), **342**, 439–468 (1993).

[12] Fraser, W.B., Ring Spinning, *TEXTILE HORIZONS*, April/May 1996, 37-39.

[13] Fraser, W. B., Clark, J. D., Ghosh, T .K., and Zeng, Q., The effect of a control ring on the stability of the ring-spinning balloon, *Proc. R. Soc. Lond.* A, (Proceedings: Mathematical, Physical and Engineering Sciences), **452**, 47–62 (1996).

[14] Fraser, W. B., Farnell, L., and Stump, D. M., Effect of yarn non-uniformity on the stability of the ring-spinning balloon, *Proc. R. Soc. Lond.* ***A,*** (Proceedings: Mathematical and Physical Sciences), **449**, 597–621 (1995).

[15] Fraser, W.B., Farnell, L. and Stump D.M., The effect of slubs on the stability of the ring-spinning balloon, *J. Textile Inst*. **86**, 610–634 (1995).

[16] Fraser, W. B., Ghosh. T. K., and Batra, S. K., On unwinding yarn from a cylindrical package", *Proc. R. Soc. Lond. A,* **436**, 479–498 (1992).

[17] Fraser, W. B. and Stump, D. M., Yarn twist in the ring-spinning balloon, *Proc. R. Soc. Lond. A,* **454**, 707–723 (1998).

[18] Mathews, A., and Hardingham, M., "Medical and Hygiene Textile Production", Intermediate Technology Publications, London, 1994.

[19] Przybyl, K., Influence of yarn defects on its tension during the spinning process on a ring spinning machine, *Fibres & Textiles in Eastern Europe*, **8**(1), 21–25 (2000).

[20] Przybyl, K., Simulating the dynamics of the twisting-and-winding system of the ring spinning frame, *Fibres & Textiles in Eastern Europe*, **9**(1) 16–19 (2001).

[21] Przybyl, K., Stability of working conditions of the twisting-and-winding system of the ring spinning frame in dependence on yarn material, *Fibres & Textiles in Eastern Europe*, **9**(4), 24–27 (2001).

[22] Przybyl, K., Influence of yarn surface properties on the dynamic of the twisting-and-winding system of the ring spinning frame, *Fibres & Textiles in Eastern Europe*, **10**(2), 27–31 (2002).

[23] Skenderi, Z., Oreskovic, V., Peric, P., and Kalinovcic, H., Determining yarn tension in ring spinning, *Textile Res. J.* **71**(4), 343–350 (2001).

[24] Stalder, H., Ring-spinning advance, *Textile Asia*, March 2000, 43–46.

[25] Tang, Z. X., Fraser, W. B., and Wang, X., Minimising energy-consumption of yarn winding in ring spinning, *Textile Res. J.* **74**(12), 1097-1103 (2004)..

[26] Tang, Z. X., Wang, X., and Fraser, W. B., Distribution of power requirements during yarn winding in ring spinning, *Textile Res. J.* **74**(8), 735–741 (2004).

[27] Tang, Z. X., Wang, X., and Fraser, W. B., Skin friction coefficient on yarn package surface in ring spinning, *Textile Res. J.* **74**(10), 845-850 (2004)

[28] Tang, Z. X., Wang, X., and Fraser, W. B., An experimental investigation of yarn tension in simulated ring spinning, *Fibers and Polymers*, (Accepted for publication).

[29] Wang, X., Effect of Testing Speed on the Hairiness of Ringspun and Sirospun Yarns, *J. Textile Inst*. **88** Part 1, No 2, 99–106 (1997).

[30] Wang, X., Measuring the Hairiness of a Rotor Spun Yarn on the Uster Tester 3 at Different Speeds, *J. Textile Inst.* **89** Part 1, No 2, 281–288 (1998).

[31] Wang, X., Testing the Hairiness of a Rotor Spun Yarn on the Zweigle G565 Hairiness Meter at Different Speeds, *J. Textile Inst*. **89** Part 1, No 1, 167–169 (1998).

[32] Wang, X., Recent Research on Yarn Hairiness Testing and Hairiness Reduction – Part 1: Hairiness Testing, *Res. Journal of Textiles and Apparel*, **2**(1), 13–20 (1998).

[33] Wang, X., and Chang, L., An Experimental Study of the Effect of Test Speed on Yarn Hairiness, *Textile Res. J.* **69**(1), 25–29 (1999).

[34] Wang, X., Huang, W., and Huang, X., Effect of Test Speed and Twist Level on the Hairiness of Worsted Yarns, *Textile Res. J.* **69** (12), 889–892 (1999).

[35] Wang, X., and Miao, M., Reducing Yarn Hairiness with an Air Jet Attachment during Winding, *Textile Res. J.* **67**(7), 481–485 (1997).

[36] Wang, X., Miao, M., and How, Y., Studies of JetRing spinning – Part 1: Reducing yarn hairiness with the JetRing, *Textile Res. J.* **67**(4), 253–258 (1997).

[37] Zhu, R., and Ethridge, M. D., Predicting hairiness for ring and rotor spun yarns and analyzing the impact of fiber properties, *Textile Res. J.* **67**(9), 694–698 (1997).

[38] Zhu, F., Hall, K., and Rahn, C. D., Steady state response and stability of ballooning strings in air, *Int. J. Non-linear Mechanics*, **33** (1), 33–46 (1998).

[39] Zhu, F., Sharma, R., and Rahn, C. D., Vibrations of ballooning elastic strings, *J. Appl. Mech.* **64**, 676–683 (1997).

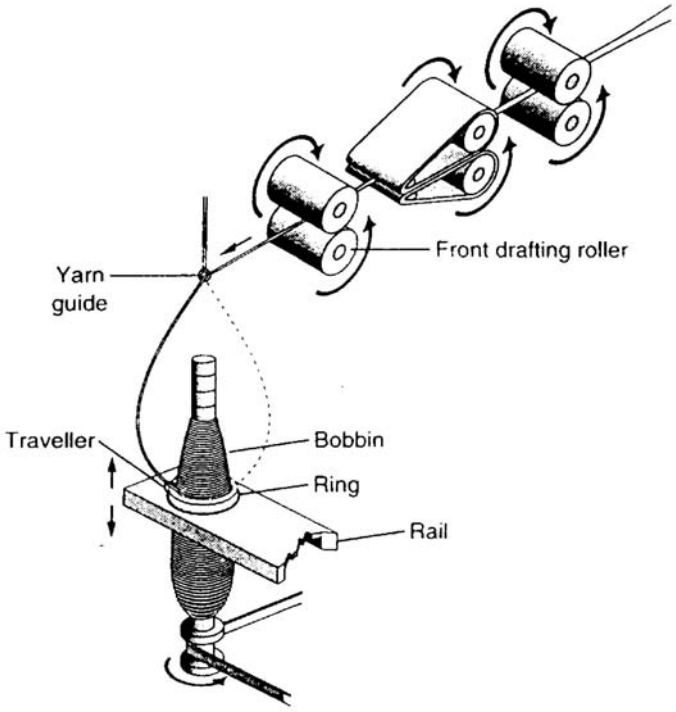

Figure 1. The ring spinning process [18].

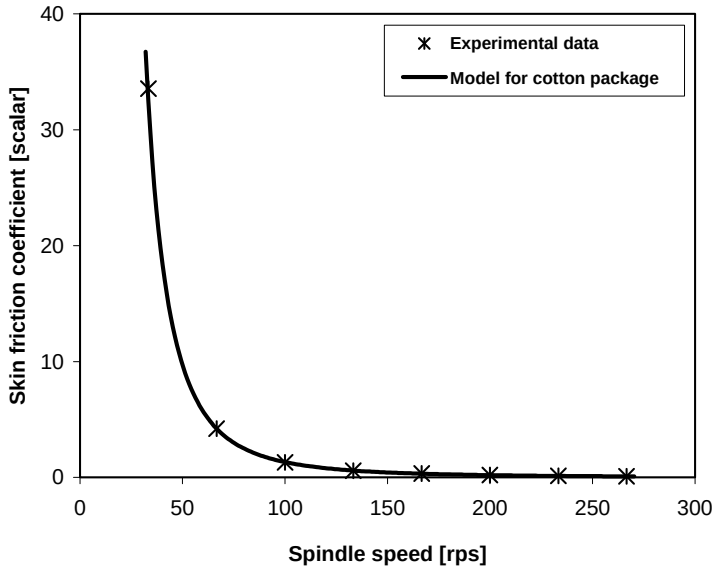

Figure 2. Modelling skin friction coefficient on the surface of a rotating natural cotton yarn pacakge (package diamter = 0.0279m).

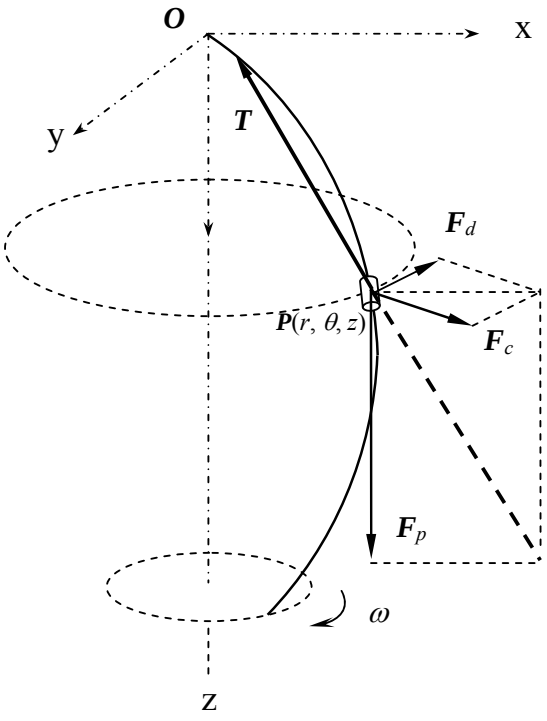

Figure 3. Yarn tension $\boldsymbol{T}$, drawing force $\boldsymbol{F}_p$, air drag $\boldsymbol{F}_d$ and centrifugal force $\boldsymbol{F}_c$ acting on a material point $\boldsymbol{P}$ on a ballooning yarn in a free-balloon ring spinning.

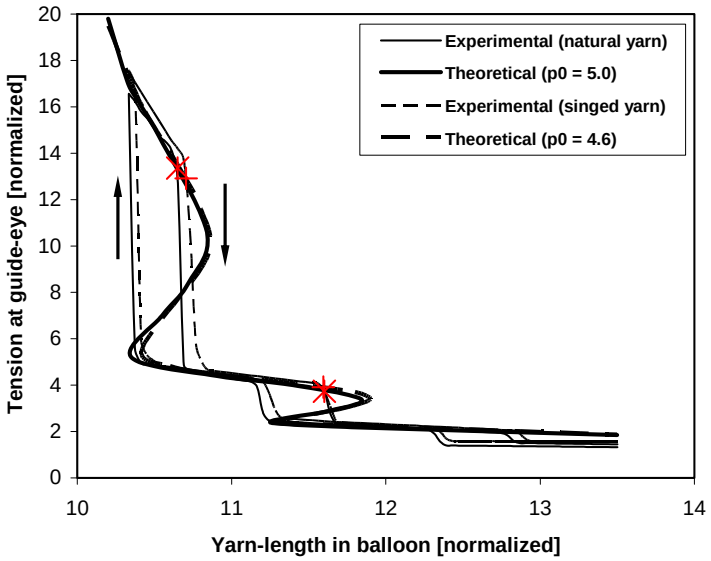

Figure 4. Modelling air drag coefficients (p_0) on ballooning 38 tex cotton yarn at 5300 rpm: $p_0 = 5.0$ for natural yarn and $p_0 = 4.6$ for singed yarn.

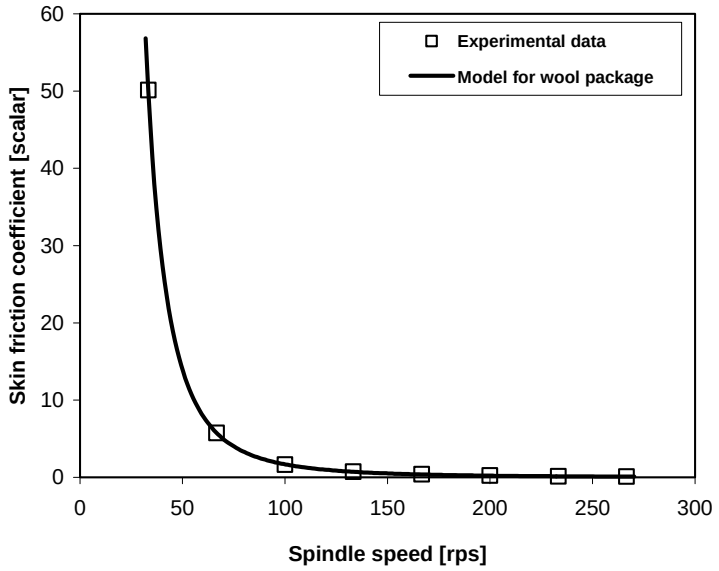

Figure 5. A comparison of skin friction coefficients on the surface of wool yarn packages between experiment and model prediction.

Figure captions

Figure 1. The ring spinning process [18].

Figure 2. Modelling skin friction coefficient on the surface of a rotating natural cotton yarn package (package diameter = 0.0279 m).

Figure 3. Yarn tension $\boldsymbol{T}$, drawing force $\boldsymbol{F}_p$, air drag $\boldsymbol{F}_d$ and centrifugal force $\boldsymbol{F}_c$ acting on a material point $\boldsymbol{P}$ on a ballooning yarn in a free-balloon ring spinning.

Figure 4. Modelling air drag coefficients (p_0) on ballooning 38 tex cotton yarn at 5300 rpm: $p_0 = 4.6$ for natural yarn and $p_0 = 5.0$ for singed yarn.

Figure 5. A comparison of skin friction coefficients on the surface of wool yarn packages between experiments and model prediction.